

Soft ion impact for surface activation during diamond chemical-vapor deposition on diamond and silicon

Kungen Teii*

Department of Applied Science for Electronics and Materials, Interdisciplinary Graduate School of Engineering Sciences, Kyushu University, 6-1 Kasuga Park, Kasuga, Fukuoka 816-8580, Japan

(Received 27 February 2001; revised manuscript received 26 June 2001; published 11 September 2001)

Extremely low-energy ions with a mean kinetic energy of around 2 eV have been used for surface activation during diamond chemical-vapor deposition at a pressure of 20 mTorr in an inductively coupled plasma. A qualitative model based on a current balance between a positively biased substrate and a surrounding wall was given to describe the variation of ion energy and flux onto the substrate. The deposits with polycrystalline morphologies were obtained on the biased diamond(100) and Si(100) substrates by varying the ion flux. The ion-enhanced surface migration of hydrocarbon adatoms was demonstrated by the ion flux dependent morphologies of diamond films grown on diamond. A high ion flux resulted in large interisland distance and island size, a low island density, and a low fraction of grain boundary. In contrast, the concurrently induced disadvantage like surface defects and etch pits was shown by the ion flux dependent morphologies of nanocrystalline diamonds grown on Si. A high ion flux resulted in nonfaceted crystallites and a high frequency of secondary nucleation. Comprehensive discussion on the role of low-energy ions in the growth kinetics suggests that soft ion impact is promising for modifying thermally dominated behaviors of adsorbed radicals and exploring simple processes.

DOI: 10.1103/PhysRevB.64.125327

PACS number(s): 68.49.Sf

I. INTRODUCTION

Conventional research for diamond chemical-vapor deposition (CVD) at relatively high system pressures on the order of $10^1 - 10^2$ Torr has commonly aimed at the fabrication of high-quality diamond on a low-cost foreign substrate such as silicon, that meets practical needs in the light of industrial applications of diamond to electronic devices. The bias-enhanced nucleation (BEN) technique¹ developed in the early 1990s has achieved high nucleation density and highly oriented nucleation and growth on such a heterogeneous substrate by applying a negative substrate direct current (dc) bias at the initial deposition stage typically in a microwave discharge plasma. However, underlying basic mechanisms of diamond deposition have not been thoroughly understood due to the high-pressure conditions, where the complex reactions in the plasma bulk and boundary layer or collisional sheath obstruct direct interpretation of observed phenomena in terms of theoretical considerations. It is plausible to assert that *simple* low-pressure conditions are highly desired for diagnostics and precise control of elementary processes, as in the case of other semiconductor materials like epitaxial silicon and III-V compounds.

Low system pressures on the order of $10^{-2} - 10^{-1}$ Torr have been employed to deposit diamond only in a small number of studies, mostly for practical purposes such as low-temperature growth and large-area coating.^{2,3} It is believed that the difficulties in depositing diamond at such low pressures lie in a high ion-bombardment energy as well as a low radical density. Accordingly, the most emphasis of the research objectives should be put on the role of radical flux and ion bombardment in the deposition. In particular, the ion-induced dynamic effects are the principal characteristics in the low-pressure deposition. The initial works by Wei *et al.*

and Eddy *et al.* revealed that a positive substrate bias was required to avoid strong ion bombardment and obtain faceted diamond in high-density microwave plasmas at $10 \sim 100$ mTorr.^{2,3} The subsequent works by Hatta *et al.* examined the temporal or time-averaged variations of radical densities during diamond growth with applying a positive substrate bias in pulse-modulated microwave plasmas at 100 mTorr.⁴ The recent works by Teii and Yoshida revealed that an ion-bombardment energy as low as 2 eV only allowed faceted diamond growth and a high ion flux relative to radical flux as well as a low radical density caused the growth suppression in high-density radio-frequency (rf) plasmas at $10 \sim 80$ mTorr.⁵ Any of these studies tends to prefer the avoidance of ion bombardment over the use of it. To the contrary, the use of ion bombardment has been typically found in the preceding BEN technique,⁶ although the decisive role of ion-induced effects in the nucleation promotion has not been fully confirmed due to the complex high-pressure conditions. In fact, the impinging ion energy has been suggested very extensively from 5 to 80 eV (Refs. 7–9) in conjunction with corresponding various mechanisms such as surface migration, discharge change, subplantation, and thermal spike. Again, *simple* low-pressure conditions should be desirable for the development of ion-assisted deposition technique because of readily definable ion energy and flux.

In this study, the deposition of diamond on single crystalline diamond and silicon substrates is performed at 20 mTorr under low-energy ion bombardment by inductively coupled plasma (ICP) enhanced CVD. A previous study showed that the ion flux bombarding a substrate during diamond growth in an ICP can be controlled at a constant ion energy of around 2 eV by positively biasing the substrate.¹⁰ In Sec. III A, a detailed analysis for the ion flux during the biasing is made based on a current balance between the substrate and reactor wall. In Sec. III B and C, the deposition on diamond

and silicon substrates is performed by varying the ion flux with the sheath potential (V_{sheath}) kept at 2 V. In Sec. III D, comprehensive discussion on the role of low-energy ion bombardment is presented. The present ion energy (\sim several eV) is much lower than the threshold (≥ 30 eV) for subplantation of carbon ions into tetrahedrally coordinated a -C films,¹¹ and just corresponds to the intermediate of a non-biased substrate and a negatively biased substrate in BEN at typical high pressures. Such low-energy ions are expected to introduce soft dynamic effects into thermally dominated behaviors of radicals through the interactions with surface atoms without bulk damage. The results should give definitive insights into the basic mechanisms of diamond CVD under low-energy ion bombardment.

II. EXPERIMENTAL DETAILS

An experimental setup has been described in detail previously.⁵ The ICP source consisting of a 6-cm-diam two-turn helical copper coil wound around a 4-cm-diam water-cooled Pyrex tube was placed on a grounded stainless steel reactor of 23 cm in diameter and 32 cm in height. The substrate holder was located downstream at about 10 cm below the source. The gas mixture of 5% CO-5% CH₄-90% H₂ with a total flow rate of 50 sccm was fed into the reactor by using mass flow controllers from the top of the ICP source. The rf plasma power at 13.56 MHz and total pressure were maintained at 1500 W and 20 mTorr, respectively. Prior to deposition, the p -type Si(100)20×20×0.6 mm substrate was scratched with diamond powder (40–60 Å) diluted in ethanol in an ultrasonic bath, followed by a rinse in ethanol and distilled water to remove residue, while the diamond (100)3×3×0.5 mm substrate (Sumitomo Electric Industries Co.) was solely cleaned in acetone in an ultrasonic bath. The use of two types of substrates with different pretreatments and surface-free energies should be helpful to understand the growth kinetics. During deposition, the substrates were mounted on a stainless steel holder and fixed with a molybdenum 50×50×0.5 mm frame cover to which a positive dc bias (V_b) was applied with respect to the grounded reactor. The chemical vapor deposited diamond is usually electrically conductive due to a H-terminated surface.¹² The substrate temperature, which was controlled by an external tantalum wire heater, was measured by a thermocouple attached to the substrate backside and kept at 770 °C.

The surface morphology of the deposits was examined by using a field emission scanning electron microscope (SEM) and an atomic force microscope (AFM). The as-grown deposits showed minor charging effects, so no coating was made prior to SEM observation. The SEM specimens were fixed on an Al holder using Ag paste at a beam-tilt angle of 30° with respect to the normal surface during observation. AFM was performed in tapping mode with a single crystalline silicon as the force sensor tip in atmosphere at room temperature. The structure and chemical bonding nature of the deposits were examined by micro-Raman spectroscopy using Ar⁺ laser radiation with 514.5 nm excitation with a wave number resolution of about 0.5 cm⁻¹ and x-ray photoelectron spectroscopy (XPS) using Mg $K\alpha$ radiation (1253.6

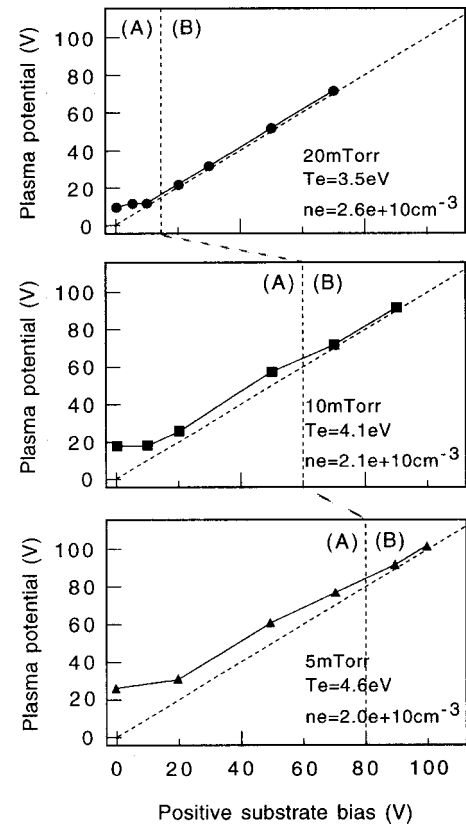


FIG. 1. Plasma potential (V_p) at 15 mm above the substrate as a function of substrate bias (V_b) at pressures of 5–20 mTorr. The two regions (A) and (B) correspond to $V_{\text{sheath}} \geq 2$ V and $V_{\text{sheath}} = 2$ V, respectively.

eV) with an energy resolution of about 0.2 eV. Angle resolved XPS spectra were obtained by varying photoelectron take-off angle (θ), defined from the parallel to the specimen surface, in the range of 30°–90°. For example, $\theta = 30^\circ$ is a surface sensitive condition. The plasma potential (V_p) was measured by using an emissive probe with a tantalum filament with an emissive area of about 9.4 mm², to determine the sheath potential $V_{\text{sheath}} = V_p - V_b$. The electron density (n_e) and temperature (T_e) at 15 mm above the substrate were measured by using a single Langmuir probe with a tantalum probe tip with a collecting area of about 3.9 mm². Details of the probe measurements have been described previously.¹³

III. RESULTS AND DISCUSSION

A. Ion energy and flux bombarding a positively biased substrate

The dependence of V_p at 15 mm above a substrate upon V_b at pressures of 5–20 mTorr is shown in Fig. 1. At the process pressure (20 mTorr), the thickness of the sheath over the substrate is found to vary with V_b from around 0.2 mm to around 0.04 mm, depending on V_{sheath} . These values are smaller than the mean-free path of ions (~ 1.5 mm). A mean kinetic energy of ions onto a substrate is therefore well described by V_{sheath} . In Fig. 1, the variations of V_p by applying

V_b are categorized into the two regions; (A) for low V_b, V_p increases with depressing V_{sheath} , (B) for high V_b, V_p increases in proportion to V_b with retaining a minimum V_{sheath} of 2 V. In addition, a critical V_b value above which V_{sheath} reaches the minimum is increased when the pressure is reduced. This is due to an increase in T_e and thereby enhanced nonequilibrium as discussed below. A shift up of V_p is due to the electrically floated characteristic of the ICP source.¹⁴ V_b usually cannot exceed V_p when the ratio of the surrounding wall area to substrate area S^w/S^s (≈ 100 in the present study), is not large enough as compared to $\sqrt{m_i/m_e} \approx 100-1000$ (m_i, m_e : ion and electron mass). A simplified explanation for this has been given based on asymmetric double probe current-voltage (I - V) characteristics in the previous study.¹⁰ The concluding remark was that, in region (B), the ion flux decreases with increasing V_b , while the ion energy remains constant at around 2 eV. This has also been confirmed experimentally by using a mass spectrometer.¹⁵ Here a detailed analysis for the ion flux during the biasing is presented.

The current balance at the substrate and grounded wall during the biasing is given by

$$(i_e^s - i_i^s)A^s = (i_i^w - i_e^w)A^w \approx i_i^w A^w, \quad (1)$$

where the superscripts s and w represent the values for the substrate holder and wall, i_e and i_i the electron and ion current density, respectively, and A the effective current collecting area of the surrounding sheath. The term i_e^w in Eq. (1) is precluded because of its small contribution. Note that A^s and A^w increase with increasing $V_{\text{sheath}} = V_p - V_b$ and V_p , respectively, due to the spherical expansion of the sheath particularly at the edge of the geometric projections. Assuming the Maxwell-Boltzmann distribution for electron velocity, the term i_e^s is expressed by

$$i_e^s = i_{e0}^s \exp\left[-\frac{e(V_p - V_b)}{kT_e}\right] \quad (2)$$

and

$$i_{e0}^s = \frac{1}{4} n_e e \sqrt{\frac{8kT_e}{\pi m_e}}, \quad (3)$$

where i_{e0}^s is the electron saturation current density, e the elementary electron charge, and k the Boltzmann constant. Further, i_i^w is related to the potential gradient from the ICP source to the vicinity of the wall by Ohm's law $\mathbf{i}_i^w \approx -\sigma \nabla V_p$, where σ is the electrical conductivity. If the local V_p over the substrate shifts up with V_b while that in the vicinity of the wall does not, ∇V_p increases with V_b . However, the radial and axial distributions of V_p for the variation of V_b indicated that an increase in V_b raises the overall V_p in the reactor, so ∇V_p and hence i_i^w are almost independent of V_b . The dependence of A^w upon V_b mainly determines the variation of ion flux onto the substrate, $i_i^s A^s/S^s$. Consequently, in region (A), the ion energy decreases with V_b due to a decrease in V_{sheath} , while the ion flux little changes. In region (B), only the ion flux decreases with V_b due to an increase in A^w , while the ion energy remains constant.

The principal qualitative success of the model described above lies in its ability to predict the effects of T_e and S^w/S^s . First, the value of T_e greatly influences the dependence of V_p upon V_b . Equations (2) and (3) reveal that both i_e^s and i_{e0}^s tend to increase with increasing T_e . To satisfy Eq. (1), V_{sheath} increases to suppress i_e^s unless V_p is high enough to yield a necessary large A^w . As T_e is increased by lowering the pressure, region (B) starts at higher V_p and hence V_b to increase V_{sheath} as shown in Fig. 1. Second, the value of S^w/S^s is closely related to the bombarding ion energy and flux. The minimum V_{sheath} achieved in region (B) is determined so as to satisfy Eq. (1), which is approximated as $A^w/A^s \approx i_e^s/i_i^w$. An increase in A^w/A^s ($\approx S^w/S^s$) corresponds to an increase in i_e^s/i_i^w . This indicates that the minimum V_{sheath} decreases to increase i_e^s when S^w/S^s is increased. On the other hand, Eq. (1) shows that the bombarding ion flux $i_i^s A^s/S^s = (i_e^s A^s - i_i^w A^w)/S^s$, is proportional to $-A^w/S^s$ ($\approx -S^w/S^s$) in region (B), where i_e^s , A^s , and i_i^w are independent of V_b . This means that the ion flux decreases when S^w/S^s is increased. Overall, a large S^w/S^s provides low-energy and flux bombardment, while a small S^w/S^s high-energy and flux bombardment, vice versa.

Now, let us consider the possibility of numerical solution for the bombarding ion flux $i_i^s A^s/S^s = (i_e^s A^s - i_i^w A^w)/S^s$ in region (B). Since i_e^s , A^s , and i_i^w are independent of V_b , $i_i^s A^s/S^s$ simply depends upon a geometrical parameter A^w , which varies with V_p . Only if we could know the dependence of A^w upon V_p or V_b , $i_i^s A^s/S^s$ would be obtained. Another better way to determine $i_i^s A^s/S^s$ is the fitting of $(i_e^s - i_i^w)A^s$ to the measured substrate I - V curve in region (B) with an approximation of $A^s \approx S^s$, a theoretical i_e^s term, and measurable other terms. The measured I - V curves in the present study were too distorted to be fitted due to the rf modulation of the plasma potential. The successful I - V measurements need to avoid the influence of rf perturbation and identify a small i_i^s against a large i_e^s .

B. Growth on diamond

Plane-view SEM images of the diamond films grown on diamond substrates at $V_b = 20$ and 50 V after a duration of 6 h are shown in Figs. 2(a) and 2(b), respectively. The ion flux is lowered from (a) to (b) at a constant V_{sheath} of 2 V. In both cases, the film thickness is around 300 nm, corresponding to the growth rate of approximately 50 nm/h. The films have polycrystalline morphologies and consist of faceted crystallites with irregular sizes of a few hundreds of nm and numerous small pits. The dramatic effects of variant ion fluxes are shown by the difference in the average size of the crystallites; the size with a high ion flux [Fig. 2(a)] is apparently larger than that with a low ion flux [Fig. 2(b)]. In addition, the crystallites with a high ion flux are well coalesced so that the grain boundaries are hardly visible. Cross-section SEM images revealed that the crystallites had columnar structures without successive secondary nucleation unlike in the case of Si substrates as shown in the next section. AFM images of

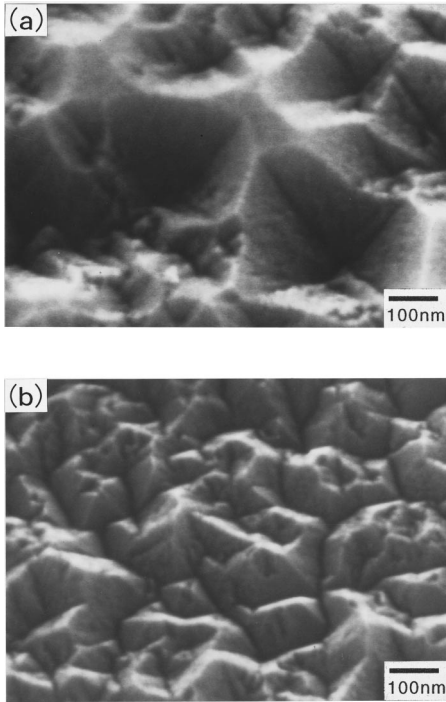


FIG. 2. SEM images of the films obtained on diamond substrates with $V_{\text{sheath}}=2$ V after a duration of 6 h; (a) high ion flux ($V_b=20$ V) and (b) low ion flux ($V_b=50$ V).

the initial diamond substrate and films corresponding to Figs. 2(a) and 2(b) for a selected area of 1000×1000 nm are shown in Figs. 3(a)–3(c). The images clearly demonstrate the evolution of crystal hill rocks or islands of several tens of nm in height on a very smooth pristine surface with a significant increase in the surface roughness regardless of exposed ion flux level. The AFM images were analyzed to obtain the root-mean-square (r.m.s.) roughness, defined by $[\sum(Z_i - Z_{\text{ave}})^2/N]^{1/2}$ where Z_{ave} is the average of the Z height values within a given area, Z_i the current Z value, and N the number of points within the selected area. The r.m.s. roughness for Figs. 3(a), 3(b), and 3(c) was estimated as around 0.7, 31, 13 nm, respectively, which had a similar trend to the peak-to-peak roughness. The present trend in the crystallite size and r.m.s. roughness for the change in ion flux is opposed to typical diamond CVD on Si in a microwave plasma where an increase in ion bombardment leads to a decrease in the crystallite size and r.m.s. roughness.¹⁶

The nucleation of an overlayer on a substrate occurs with no potential barrier if the wetting condition is satisfied¹⁷

$$\gamma_s \geq \gamma_o + \gamma_i, \quad (4)$$

where γ is the surface free energy and the subscripts s , o , and i correspond to the substrate, overlayer, and interface, respectively. This is the criterion for layer-by-layer growth (Frank-van der Merwe, 2D mode) rather than island growth (Volmer-Weber, 3D mode). The polycrystalline film morphologies are indication of island growth, although one may expect layer-by-layer growth because the use of a homogeneous substrate could often satisfy the wetting condition as seen in typical homoepitaxial growth of diamond. The mode

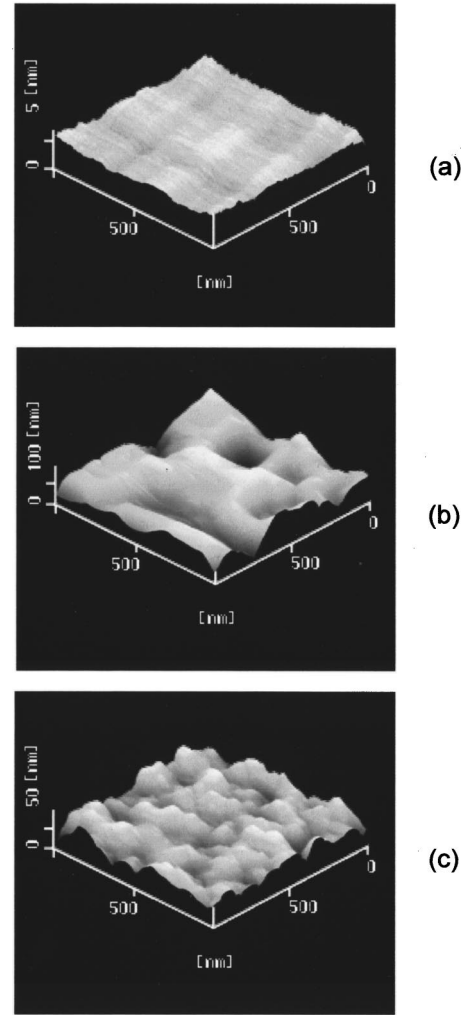


FIG. 3. AFM images of (a) the initial diamond substrate and the films obtained on diamond substrates with $V_{\text{sheath}}=2$ V after a duration of 6 h; (b) high ion flux ($V_b=20$ V); and (c) low ion flux ($V_b=50$ V).

transition from layer-by-layer growth to island growth depends upon the free energy for the condensation.¹⁸ As the variation of the free energy at the transition from the vapor to the solid phase decreases with decreasing supersaturation, island growth is energetically favored, since the formation enthalpy of 3D nuclei is more than that of 2D nuclei. The supersaturation depends on the incident flux of condensing atoms (or hydrocarbon radicals) at a given substrate temperature. The degree of supersaturation is relatively low in the low-pressure growth condition, the resulting films therefore have polycrystalline morphologies.

C. Growth on silicon

Plane-view SEM images of the diamond crystallites grown on Si substrates at $V_b=20$ and 50 V after durations of 3, 6, and 9 h are shown in Figs. 4(a)–4(f). The two sets of series, (a)–(c) and (d)–(f), show the temporal change in the surface morphology for $V_b=20$ and 50 V, respectively. The ion flux is lowered from (a)–(c) to (d)–(f) at a constant

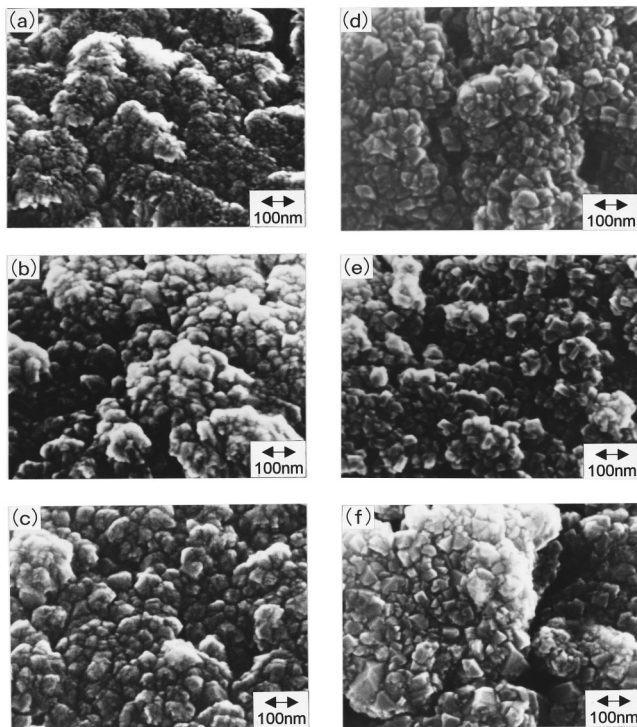


FIG. 4. SEM images of the deposits obtained on Si substrates with $V_{\text{sheath}} = 2$ V; after durations of (a) 3, (b) 6, and (c) 9 h for a high ion flux ($V_b = 20$ V), and after durations of (d) 3, (e) 6, and (f) 9 h for a low ion flux ($V_b = 50$ V).

V_{sheath} of 2 V. The deposits are composed of fine crystallites with sizes of several tens of nm, all of which are coalesced into spherical islands with sizes of a few hundreds of nm. The islands are occasionally further coalesced into segmented films with sizes of a few μm . It is possible to confirm the existence of crystal facets, a characteristic of diamond, for the low flux series [(d)–(f)]. But it is not for the high flux series [(a)–(c)] probably due to a high density of surface defects and etch pits. The coalesced morphology is an indication of a high frequency of secondary nucleation on the primary crystallite surfaces, and the island density is considered to represent the actual nucleation density. The nucleation density showed a slight tendency to decrease with increasing duration from 3 to 9 h due to the progress of coalescence. It increased from around $7 \times 10^9 \text{ cm}^{-2}$ at $V_b = 20$ V to around $1 \times 10^{10} \text{ cm}^{-2}$ at $V_b = 50$ V with decreasing ion flux. Despite the low reproducibility and uniformity of nucleation density over an entire surface of a scratched Si surface, the trend is consistent with the correlation between the ion flux and island density discussed in the next section. As a duration increases, the average island size increases due to the successive nucleation. Despite a distribution of the crystallite sizes, it is interesting to note that a duration exceeding 3 h results in only a little increase in the overall crystallite sizes. The maximum grain (crystallite) size roughly estimated from the SEM images as a function of duration is shown in Fig. 5. The error in the size estimation was less than 15 nm, and the measurable size limit was as small as 10 nm. The size increases for duration up to 3 or 6

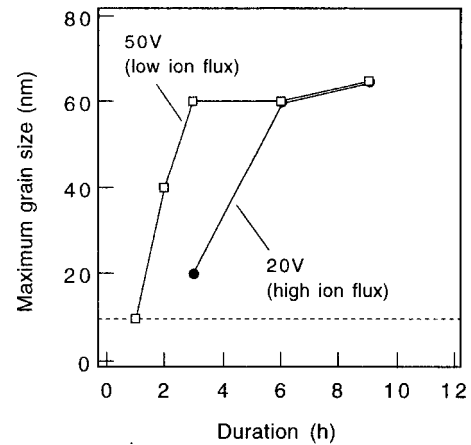


FIG. 5. Maximum grain size as a function of duration for a high ion flux ($V_b = 20$ V) and a low ion flux ($V_b = 50$ V). The dashed line represents the smallest size (≈ 10 nm) measurable from the SEM images.

h for the low or high flux series, respectively, and exhibits a tendency to saturation at around 60 nm. A similar result has been obtained in almost equivalent conditions with low-energy ions¹⁹, where the sizes were saturated at around 20 nm for duration up to 20 h.

Micro-Raman spectra for the deposits at $V_b = 20$ –70 V after a duration of 3 h are shown in Fig. 6. The ion flux is lowered with increasing V_b . Any of these spectra exhibits a cubic diamond peak at 1328 – 1330 cm^{-1} , which is superimposed on a feature from sp^2 -bonded amorphous carbon at around 1350 cm^{-1} , corresponding to the D line associated with disorder-allowed zone-edge modes of graphite. The presence of a diamond peak will be more clearly distinguished when one uses an excitation laser beam with shorter wavelengths to suppress the background.²⁰ The spectra also exhibit a broad peak from sp^2 -bonded amorphous carbon at 1500 – 1550 cm^{-1} , corresponding to the G line associated with optically allowed E_{2g} zone center mode of graphite. The diamond peak somewhat shifts to lower wave numbers as compared to 1332 cm^{-1} normally observed for natural

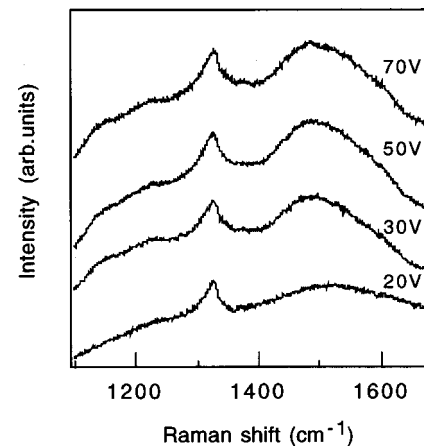


FIG. 6. Raman spectra for the deposits obtained on Si substrates with $V_{\text{sheath}} = 2$ V after a duration of 3 h. An increase in V_b from 20 to 70 V corresponds to a decrease in ion flux.

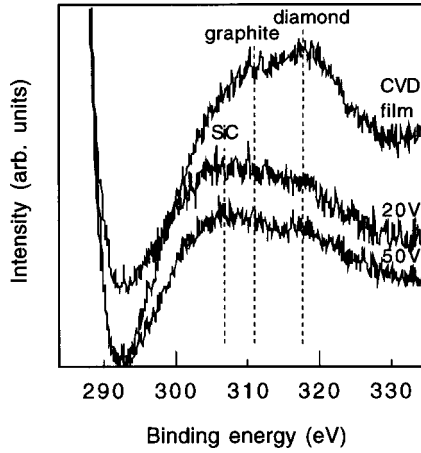


FIG. 7. Valence band XPS spectra of $C1s$ at $\theta=30^\circ$ for the deposits obtained on Si substrates with $V_{\text{sheath}}=2$ V ($V_b=20$ and 50 V) after a duration of 3 h and a typical diamond film by microwave plasma CVD. Typical assignments for the plasmon energy of silicon carbide, graphite, and diamond are given by the dashed lines.

diamond and has a broad and asymmetric line shape due to phonon scattering from the boundaries of the Brillouin zone, typical for nanocrystalline diamond.²¹ A decrease in ion flux by increasing V_b little influences the diamond peak despite the difference in the crystallite sizes (20–70 nm), suggesting that the effective domain sizes for Raman scattering were identical due to the coalescence. Instead, it causes a slight increase in the amount of amorphous carbon relative to diamond, as the ratio of the G line to diamond peak intensities increases from 0.96 at $V_b=20$ V to 1.05 at $V_b=70$ V. This indicates that a high ion flux more efficiently removed the codepositing nondiamond carbon phase.

A complementary proof for diamond phase is given by plasmon loss features in valence band XPS spectra of carbon. Figure 7 compares the $C1s$ spectra for the deposits at $V_b=20$ and 50 V after a duration of 3 h with that for a typical microwave plasma deposited diamond film over $1 \mu\text{m}$ thick on Si. The bulk plasmon loss is often used as the measure of number density of atoms by assuming a free-gas model for valence electrons.²² The bulk plasmon energy (E_p) is measured from the main peak energy and related to the local valence electron density (n) by

$$E_p = \hbar \left(\frac{ne^2}{\epsilon m_{em}} \right)^{1/2}, \quad (5)$$

where m_{em} the effective mass of electrons and \hbar and ϵ have their original meanings. For example, the measured E_p of diamond is usually seen at around 33 eV, while that of graphite and silicon carbide at around 27 and 23 eV, respectively. The spectrum for a typical CVD film exhibits the bulk plasmon for diamond and graphite with a weak shoulder at 22–24 eV due to either the SiC component or the surface plasmon for diamond. The spectra at $V_b=20$ and 50 V have a broad peak at 22–24 eV with some tailing toward a high-energy side, in addition to the bulk plasmon for diamond. One cannot distinguish between the SiC and graphitic carbon contributions in the spectra.

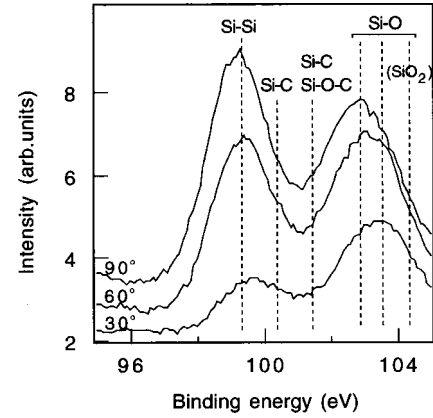


FIG. 8. Angle resolved XPS spectra of $S2p$ at $\theta=30^\circ-90^\circ$ for the deposits obtained on Si substrates with $V_{\text{sheath}}=2$ V ($V_b=20$ and 50 V) after a duration of 3 h. Typical assignments for the binding energy of possible bonding components are given by the dashed lines.

Further information on bonding components at the interface is obtained by chemical shifts in angle resolved XPS core-level spectra of silicon. The Si $2p$ spectra for the deposits at $V_b=50$ V after a duration of 3 h are shown in Fig. 8. The spectra at $V_b=20$ V were almost equivalent. The possible bonding components are assigned as bulk Si-Si (99.3 eV), interface Si-C (100.3 eV), bulk Si-C or Si-O-C (101.4 eV), and bulk Si-O (102.7–104.3 eV). The energy variation for Si-O bonds corresponds to the difference in the bonding properties. The spectra before deposition (not shown) consisted of two major peaks arising from elemental silicon and native oxide. After deposition, the two peaks tend to exhibit chemical shifts to higher binding energies especially at low θ . The interface silicon carbide is shown by an ambiguous shoulder at around 100.3 eV probably due to the small thickness. Both the Si-C and Si-O peak intensities increase relative to the Si-Si peak intensity with decreasing θ due to the carbide and oxide-rich top layer. Thus the present interface structure is likely equivalent to the typical silicon-diamond interface structure described as Si/SiO/SiC/ a -C/diamond.²³ The spherical island morphologies are explained by the energetic relationship between the substrate and overlayer. The surface energy of 5.3 J m^{-2} for diamond is much higher than 1.5 J m^{-2} for silicon,²⁴ while the possible interfaces have positive surface energies. The diamond nucleation on silicon is difficult, unless the nucleus or embryo has a fully hydrogenated surface which considerably lowers the surface energy.²⁵ Anyway, the low wetting ability of diamond against Si with little catalytic effect results in spherical island growth with a high contact angle.

D. Role of low-energy ion bombardment

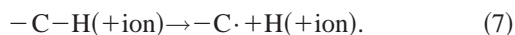
A primary role of low-energy ion bombardment corresponding to a V_{sheath} of 2 V is to enhance the migration of adatoms or small clusters. The kinetic energies of ions as low as typical interatomic binding energies (\sim several eV) are efficiently transferred upon impact at the surface from the incoming ions to the substrate atoms with minimum bulk

damage. Some energy will be distributed among the adatoms nearby, leading to a local increase in their mobilities. According to the basic theory for vacuum vapor deposition, the average migration length (\bar{X}) of diffusive adatoms prior to thermal desorption is expressed as¹⁷

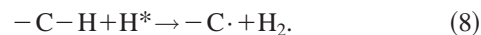
$$\bar{X} = \sqrt{D\tau} = \left[2a^2\nu\tau \exp\left(-\frac{Q_{\text{act}}}{2kT}\right) \right]^{1/2}, \quad (6)$$

where D is the diffusion coefficient, τ the residence time given by Frenkel's equation, Q_{act} the activation energy for surface migration, a the distance of a jump across a periodic potential relief with a barrier of Q_{act} , ν the vibration frequency, and T the adatom temperature, which is usually higher than the substrate temperature. The transferred energy upon impact enables the adatoms to overcome the potential barrier Q_{act} and diffuse longer across the surface as long as the desorption little changes. Thus the mechanism for the ion-enhanced migration is somewhat analog to locally increasing the adatom temperature. For example, the value of Q_{act} has been suggested as 0.7 eV and ~ 1 meV for an Al adatom on the clean and H-terminated diamond surfaces, respectively.²⁶ For some hydrocarbons, the value of Q_{act} has been suggested as 0.5–3.5 eV for a limited case of a jump between two neighboring adsorption sites (Ref. 27). The correlation between the ion flux and film morphology on diamond substrates (Fig. 2) is explained by the ion-induced migration change. A previous study by varying the ion flux (or ion-to-adatom flux ratio) in an extensive range suggested the need for optimizing \bar{X} to obtain the highest nucleation density on Si substrates.²⁸ If the migration is sufficient for efficient clustering of adatoms, the rate and density of nucleation are limited by the total flux of clustering adatoms and \bar{X} , respectively. Here we consider hydrocarbon radicals (C_xH_y) as the clustering adatoms and CH_3 as the most important growth precursors from a previous study.¹⁹ A high ion flux prolongs \bar{X} by increasing the available energy per adatom. This leads to an increase in interisland distance and island size and a decrease in island density because of an enlarged capture area of an island for diffusing adspecies. As the growth continues, the islands inhibit the formation of new islands nearby and are readily coalesced at the early stage of the growth. The resulting film consists of large grains with a low fraction of grain boundary, showing a continuous appearance. But this is not the case on Si substrates (Fig. 4), where the deposits consist of fine crystallites with a considerably high fraction of grain boundary due to the successive nucleation.

Another important role of low-energy ion bombardment is its ability to remove chemisorbed H atoms from a H-terminated diamond surface, creating available lattice sites (vacant sites) $-C\cdot$.



The physical removal process of terminal H atoms acts as an alternative pathway to the chemical abstraction process by de-excitation of gaseous excited-state H^* atoms,²⁹ typical for diamond CVD:



An increase in the number of vacant sites can increase the sticking probabilities of the growth precursors, and also the rate of diamond growth since the sites creation has been usually considered as the rate-limiting step at low system pressures with a low H flux.³⁰ One may claim that the physical process [Eq. (7)] is unlikely since the typical bond energy of C-H (≈ 4 eV) is higher than the present mean energy of ions (≈ 2 eV). Nevertheless, it is still expected since there exists a high fraction of high-energy-tail ions with high drifting energies caused by the V_p drop along the diffusing plasma stream. The drifting energy of ions prior to entering the sheath estimated from the ion energy distribution appeared to range up to 5 eV in an almost equivalent condition.²⁸ Such high-energy tails after an additional acceleration in the sheath by V_{sheath} can create undesirable surface defects as well as vacant sites on the growing diamond surfaces. On the other hand, mass spectrometry revealed that the dominant ionic species were hydrocarbons, hydrogens, and hydroxides such as CH_3^+ , CH_5^+ , H_3^+ , H^+ , H_3O^+ in similar deposition conditions.³¹ In particular, H^+ ions with a mean kinetic energy of around 2 eV are energetic and highly reactive as compared to H atoms with only a thermal energy (≤ 0.1 eV). They act as strong etchants and readily create surface defects and etch pits despite a low energy relative to an interatomic binding energy. As the ion flux increases, the enhanced creation of vacant sites is balanced by the concurrent H^+ ion etching. A combined process of deposition and etching determines the net growth rate.

The deposition on Si substrates is mainly characterized by the coalescence of the crystallites. The coalesced appearance is due to the successive secondary nucleation, and its driving force is considered to be the fluctuation of local carbon concentration on a growing diamond surface. According to the mechanism by Singh,³² once a steady-state amorphous thin layer over a diamond surface exceeds a critical thickness (≈ 15 nm) by the concentration fluctuation, the fluctuated foreign regions act as nucleation sites via recrystallization. Then the secondary diamond nuclei a few nm across embedded in the amorphous layer grow. The local transformation of amorphous or graphitic structures into diamond structures is likely caused by irradiation of ions with high kinetic energies on the order of tens to hundreds, or mega eV.^{33–35} However, such energies are much higher than the present ion energy. It may be better explained by thermodynamic effects as a consequence of exothermic and endothermic reactions such as hydrogen abstraction, termination, and recombination³⁶ rather than by ion-induced dynamic effects. The locally fluctuated regions will suffer from rearrangement of sp^2 -bonded structures towards more stable sp^3 -bonded structures by hydrogen termination to achieve the lowest surface free energy. Some of the sp^3 -bonded precursors grows into nanodiamond nuclei under the local thermodynamic conditions. In fact, a theoretical study by Badziag *et al.* showed that nanocrystalline diamonds with hydrogen terminated surfaces are energetically more stable than graphite.³⁷ Thus the present hypothesis on secondary nucleation resembles the basic capillarity theory based on thermodynamics where the embryo overcomes a specific potential barrier and stabilizes as the nucleus. The ion bombardment is considered to promote

the fluctuation of local carbon concentration by creating high-energy singular points such as surface defects, leaving an effective hold of subsequent conversion into nucleation sites. A high ion flux consequently leads to a high frequency of secondary nucleation.

Low-energy ion bombardment is thus helpful for activating the growing diamond surfaces by increasing mobilities of adatoms and creating vacant sites. The disadvantage is the most likely caused by the concurrent creation of disordered domains like surface defects and etch pits, which deteriorate crystal qualities and facilitate unnecessary secondary nucleation. Nevertheless, the advantage can be applied to modify the process window of diamond CVD and shift the phase equilibrium, which is typically dominated by temperature and mass dependent parameters of incident radicals such as excited-states, reaction efficiencies, and fluxes. In fact, a recent study has demonstrated that a low-pressure limit (≤ 10 mTorr) of diamond CVD under low-energy ion bombardment is determined by the incident fluxes of H and OH radicals and their reaction efficiencies in creating vacant sites for incorporation of hydrocarbon precursors rather than by the incident ion flux or ion-induced damage.³¹ The proper use of low-energy ions will be promising for assisting the kinetics and energetics of radicals and thereby depressing the pressure limit. It allows simple low-pressure conditions with well-controlled elementary processes eventually in atomic/molecular scale.

Due to the possible difference in the fundamental chemistries in gas phase as well as the ion and neutral fluxes onto the substrate, a comparison of the present low-pressure results with the high-pressure BEN process still needs to be considered. For example, the present ion flux estimated from T_e and n_e was less than $10^{16} \text{ cm}^{-2} \text{ s}^{-1}$, which is somewhat lower than $10^{17} \text{ cm}^{-2} \text{ s}^{-1}$ in BEN. A similarity is found in the role of ion bombardment in surface migration of adatoms. Jiang *et al.* confirmed that the interisland distance with a negative substrate bias in BEN was larger than that expected from a random nucleation model.⁶ This could prove the substantial role of low-energy ion bombardment in BEN, helping clustering and nucleation. If the ion energy in BEN is high enough or has a high-energy-tail component for subplantation (≥ 30 eV), the ion-induced effects are quite differ-

ent. In fact, nanocrystalline diamonds formed by ion-beam irradiation with high kinetic energies (80–200 eV) were shown to serve as seeds for subsequent large crystals grown by hot-filament CVD.³⁸ This apparent gap in the ion energy level strongly indicates the variety of nucleation paths. Anyway, simple conditions should help us to identify the validity of various mechanisms accounting for BEN for heteroepitaxial growth of diamond, the most intensively remarked by the researchers.

IV. CONCLUSIONS

Effects of low-energy ion bombardment on diamond growth were examined at 20 mTorr in a low-pressure ICP. From a current-balance equation for a positively biased substrate and a reactor wall, the ion flux onto the biased substrate was shown to be varied at a mean ion energy of around 2 eV. The advantage of low-energy ions was found in enhancing surface migration of adatoms through the efficient energy transfer upon impact with surface atoms. This effect was proven by the ion flux dependent morphologies of diamond films on diamond substrates, where a high ion flux resulted in large interisland distance and island size, a low island density, and a low fraction of grain boundary due to the immediate coalescence of islands. In contrast, the disadvantage was found in creating disordered domains like surface defects and etch pits the most likely by reactive H^+ ions and high-energy-tail ions with high drifting energies. This effect was confirmed by a high frequency of secondary nucleation and facetless morphologies of nanocrystalline diamonds on Si substrates. The size of the nanocrystallites had a tendency to saturation with the growth time. The results indicate that further application of low-energy ions to assisting the surface kinetics and energetics of radicals is helpful for diamond CVD at satisfactory low pressures.

ACKNOWLEDGMENTS

The author would like to thank Professor T. Goto and Associate Professor M. Hori of Nagoya University for overall supports and Dr. H. Ito of Nagoya Municipal Industrial Research Institute for AFM observation.

*E-mail address: teii@ence.kyushu-u.ac.jp

¹S. Yugo, T. Kanai, T. Kimura, and T. Muto, *Appl. Phys. Lett.* **58**, 1036 (1991).

²J. Wei, H. Kawarada, J. Suzuki, and A. Hiraki, *J. Cryst. Growth* **99**, 1201 (1990).

³C. R. Eddy, Jr., D. L. Youchison, B. D. Sartwell, and K. S. Grabowski, *J. Mater. Res.* **7**, 3255 (1992); D. L. Youchison, C. R. Eddy, Jr., and B. D. Sartwell, *J. Vac. Sci. Technol. A* **11**, 103 (1993).

⁴A. Hatta, K. Kadota, Y. Mori, T. Ito, T. Sasaki, A. Hiraki, and S. Okada, *Appl. Phys. Lett.* **66**, 1602 (1995); A. Hatta, H. Suzuki, K. Kadota, H. Makita, T. Ito, and A. Hiraki, *Plasma Sources Sci. Technol.* **5**, 235 (1996).

⁵K. Teii and T. Yoshida, *J. Appl. Phys.* **85**, 1864 (1999).

⁶X. Jiang, K. Schifmann, and C.-P. Klages, *Phys. Rev. B* **50**, 8402

(1994); X. Jiang, W. J. Zhang, and C.-P. Klages, **58**, 7064 (1998).

⁷B. R. Stoner, G.-H. M. Ma, S. D. Wolter, and J. T. Glass, *Phys. Rev. B* **45**, 11067 (1992).

⁸W. Kulisch, L. Ackermann, and B. Sobisch, *Phys. Status Solidi A* **154**, 155 (1996).

⁹J. Gerber, S. Sattel, H. Ehrhardt, J. Robertson, P. Wurzing, and P. Pongratz, *J. Appl. Phys.* **79**, 4388 (1996).

¹⁰K. Teii, *Appl. Phys. Lett.* **74**, 4067 (1999).

¹¹Y. Lifshitz, G. D. Lempert, and E. Grossman, *Phys. Rev. Lett.* **72**, 2753 (1994).

¹²H. Kawarada, H. Sasaki, and A. Sato, *Phys. Rev. B* **52**, 11351 (1995).

¹³K. Teii, *J. Vac. Sci. Technol. A* **17**, 138 (1999).

¹⁴B. A. Smith and L. J. Overzet, *Appl. Phys. Lett.* **70**, 1950 (1997).

- ¹⁵R. Nozawa, H. Takeda, M. Ito, M. Hori, and T. Goto, *J. Appl. Phys.* **81**, 8035 (1997).
- ¹⁶C. Z. Gu and X. Jiang, *J. Appl. Phys.* **88**, 1788 (2000).
- ¹⁷*Physics of Thin Films*, by L. Eckertová (Plenum, New York, 1986).
- ¹⁸K. Reichelt, *Vacuum* **38**, 1083 (1988).
- ¹⁹K. Teii, H. Ito, M. Hori, T. Takeo, and T. Goto, *J. Appl. Phys.* **87**, 4572 (2000).
- ²⁰K. Okada, H. Kanda, S. Komatsu, and S. Matsumoto, *J. Appl. Phys.* **88**, 1674 (2000).
- ²¹M. Yoshikawa, Y. Mori, H. Obata, M. Maegawa, G. Katagiri, H. Ishida, and A. Ishitani, *Appl. Phys. Lett.* **67**, 694 (1995).
- ²²T. Miyazawa, S. Misawa, S. Yoshida, and S. Gonda, *J. Appl. Phys.* **55**, 188 (1984).
- ²³D. A. Muller, Y. Tzou, R. Raj, and J. Silcox, *Nature (London)* **366**, 725 (1993).
- ²⁴*The Properties of Diamond*, edited by J. E. Field (Academic, London, 1979).
- ²⁵J. Robertson, *Diamond Relat. Mater.* **4**, 549 (1995).
- ²⁶T. Hoshino, K. Yamazaki, S. Sagiya, M. Hata, and M. Tsuda, *Phys. Rev. B* **60**, 4810 (1999).
- ²⁷K. Larsson and J.-O. Carlsson, *Phys. Rev. B* **59**, 8315 (1999).
- ²⁸K. Teii, M. Hori, and T. Goto, *J. Appl. Phys.* **89**, 4714 (2001).
- ²⁹J. C. Angus and C. C. Hayman, *Science* **241**, 913 (1988).
- ³⁰D. G. Goodwin, *J. Appl. Phys.* **74**, 6888 (1993).
- ³¹K. Teii *et al.* (unpublished).
- ³²J. Singh, *J. Mater. Sci.* **29**, 2761 (1994).
- ³³E. G. Spencer, P. H. Schmidt, D. C. Joy, and F. J. Sansalone, *Appl. Phys. Lett.* **29**, 118 (1976).
- ³⁴G. Amaratunga, A. Putnis, K. Clay, and W. Milne, *Appl. Phys. Lett.* **55**, 634 (1989).
- ³⁵P. Wesolowski, Y. Lyutovich, F. Banhart, H. D. Carstanjen, and H. Kronmüller, *Appl. Phys. Lett.* **71**, 1948 (1997).
- ³⁶M. Frenklach and K. E. Spear, *J. Mater. Res.* **3**, 133 (1988).
- ³⁷P. Badziag, W. S. Verwoerd, W. P. Ellis, and N. R. Greiner, *Nature (London)* **343**, 244 (1990).
- ³⁸W. J. Zhang, X. S. Sun, H. Y. Peng, N. Wang, C. S. Lee, I. Bello, and S. T. Lee, *Phys. Rev. B* **61**, 5579 (2000).